ACS Partner Journal

CHEM & BIO ENGINEERING

pubs.acs.org/ChemBioEng

Article

Carbazole-Bearing Conjugated Microporous Polymer Electrodes for Uranium Extraction from Seawater with Good Anti-biofouling Feature

Xinyue Zhang, Xinying Lei, Hongfei Sun, Hanming Ke, Jingxuan Xu, Yuhao Yang, Sai Zhang, Tao Wen,* Zhuoyu Ji, and Xiangke Wang*

Cite This: *Chem Bio Eng.* 2025, 2, 53−63

Read Online

ACCESS | Metrics & More | Article Recommendations | Supporting Information

ABSTRACT: Emerging electrochemical uranium extraction from seawater offers a promising route for a sustainable fuel supply for nuclear reactor operation. In this work, we intentionally synthesized a conjugated microporous polymer (CMP) with π-conjugated skeletons and permanent porosity, which was induced by in situ electropolymerization on flexible carbon cloths, followed by postdecorating amidoxime groups to create functional materials (CMP-AO). Driven by an extra asymmetrical alternating current electrochemical extraction, the self-supporting and binder-free electrode is exceptionally capable of selectively and rapidly capturing U(VI) from simulated solution, affording an extraction capacity of ∼1806.4 mg/g without saturation. Experimental observation in combination with ex/in situ spectroscopy revealed that CMP-AO enabled surface selective binding sites (amidoxime groups) to U(VI), followed by electrocatalytic reduction (carbazole groups) to yield yellow precipitates ($Na_2O(UO_3{\cdot}H_2O)_x$) via reversible electron transfer in the presence of sodium electrolyte. Furthermore, the integrating adsorption-electrocatalysis system achieved an extraction capacity of 18.8 mg/g in real seawater for 21 days and good antibiofouling abilities, validating its feasibility for practical application.

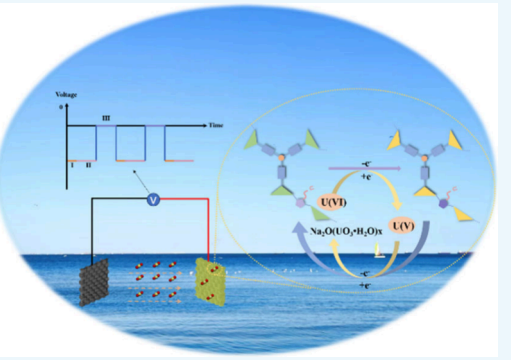

KEYWORDS: *Conjugated microporous polymer, amidoxime groups, carbazole groups, adsorption-electrocatalysis, uranium extraction*

INTRODUCTION

Limited uranium ore resources and sustained global nuclear energy requirements have motivated great interest in seeking alternative sites from unconventional resources. Uranium extraction from seawater is regarded as an emerging and promising solution for sustainable and empowering nuclear reactors. An estimated 4.5 billion tons of uranium reserves are in the ocean, which is approximately 1000× more than proven terrestrial storage.[1] This amount can afford nuclear power plant operation for thousands of years. Although the uranium reserve in seawater is massive, the ultralow concentration (approximately 3.3 ppb) and poor selectivity in a high salinity background (complexity of seawater) bring severe restrictions of uranium extraction from seawater.[2,3] Therefore, the development of technology capable of economical uranium extraction to replenish ore-based uranium resources is of great significance to provide an opportunity for a sustainable fuel supply.

In recent years, various emerging technologies have been evaluated as means of uranium extraction from seawater, such as adsorption,[4,5] chemical reduction,[6,7] photocatalysis,[8−10] electrosorption/catalysis,[11−13] etc. Physicochemical adsorption has been demonstrated to be an adaptable technique owing to its versatile, affordable, and simple to operate for attenuating uranium concentrations. Despite some progress in uranium capture, including adsorption capacity, affinity, and reusability, significant challenges faced by the majority of adsorbents are the issues of the targets for selectivity, operating time, and practical utilization. In addition to the well-established adsorption approaches, chemical reduction, photochemical, and electrochemical approaches have entered into our sight for marine uranium capture. Thanks to the advantages of fast reactions, large capacity, and insignificant pH effect, an alternative strategy to attenuate U(VI) concentration is chemical reduction of adsorbed U(VI) into sparingly soluble U(IV) using zerovalent iron nanoparticles.[7] However, metallic iron can be used mostly for heavy metal reduction. In this regard, the selective recognition and chemical reduction of adsorbed U(VI) to insoluble U(IV) and the regeneration of

Received: August 28, 2024
Revised: October 10, 2024
Accepted: October 10, 2024
Published: October 19, 2024

the active sites are of great significance for the sake of improving the uranium extraction performance. In this respect, emerging photochemical and electrochemical strategies have attracted ever-increasing attention for mining uranium from seawater. Driven by extra sunlight or by an electric field, the adsorption-reduction process controls the mass transfer diffusion of uranium from solution to the adsorbent/catalyst surface. Nonetheless, the photocatalytic technique has the drawback that large amounts of sacrificial hole scavengers are needed to restrain the fast recombination of electron−hole pairs.[14] Although some studies were reported to achieve selective uranium extraction from seawater without any sacrificial reagents, the slow kinetics and the poor stability of photocatalysts under realistic ocean circulation reduce viability as a practical uranium capture strategy.[8,15] Electrochemical uranium extraction is an effective means to solve the above issues. In particular, a half-wave rectified alternating-current electrochemical (HW-ACE) technique was adopted to guide the migration of uranyl ions to functionalized electrodes and further electrodeposition to neutralize the charged uranyl ions forming insoluble UO_2.[16] Such a HW-ACE method can alleviate Coulomb repulsion of the metal cations and selectively enrich many target ions as well as avoid water splitting. Therefore, the design and fabrication of conductive materials that synergistically combine specific sites for the binding of uranyl ions with electrocatalytic activity still remain a significant challenge.

Carbazole-bearing microporous organic polymers, which consist of organic building monomers connected by strong covalent bonds and electroactive moieties of π-conjugated skeletons, have unique advantages in the extraction of uranium.[17] Electrically driven electropolymerized organic material have been demonstrated with high conductivity and outstanding electrochemical performance.[18] Especially, N-substituted carbazole units can serve as redox-active centers. Inspired by coupling with each other to form dimeric carbazole units upon electrooxidative reaction, we can expect the construction of a conjugated microporous polymer (CMP), which was synthesized via electropolymerization between 4,4,4-tris(N-carbazolyl)-triphenylamine (TCTA) and N-(2-cyanoethyl)-pyrrole (NCP). Postsynthetically, it was functionalized with flexible amidoxime groups, showing great potential for efficient and selective uranyl adsorption. Once the UO_2^{2+} ions were bound on the electrode surface, carbazole groups served as redox-active units for the rapid reduction of the adsorbed U(VI) ions to U(V). Subsequently, unstable U(V) could be reoxidized to U(VI), giving rise to the formation of uranium compounds. Based on this discovery, a series of batch experiments were investigated with an emphasis on varying U(VI) initial concentrations, pH, applied potential, reaction time, and interfering ions. The electrochemical process exhibited much faster kinetics than that of physicochemical adsorption. By applying HW-ACE, the CMP-AO electrode was endowed with an ultrahigh uranium extraction capacity of 1806.4 mg/g without reaching saturation. The selective distribution coefficient value (K_d) of CMP-AO for uranyl ions reached 9.63×10^4 mL/g in the presence of multiple coexisting ions. Uranium extraction uptake of CMP-AO reached 18.8 mg/g after 21 days of exposure in natural seawater. Therefore, the CMP-AO framework can be in situ electropolymerized as thin film on a conductive substrate and utilized as adsorption−electrocatalyst for uranium extraction from seawater.

EXPERIMENTAL SECTION

Chemicals and Instrumentation. All chemicals are sourced from commercial suppliers and are used as received without further purification. Ultrapure water (>18.2 MΩ) was used in this study. Powder X-ray diffraction (PXRD) patterns were recorded on a Rigaku SmartLab SE X-ray diffractometer with Cu Kα radiation. Scanning electron microscopy (SEM) images and energy dispersive X-ray spectroscopy (EDS) measurements were taken with a Quattro-S scanning electron microscope. High-resolution Raman and in situ Raman spectra were obtained from CMP or CMP-AO electrodes on Raman spectrometer iHR550 equipped single-mode 532 nm diode laser. X-ray photoelectron spectroscopy (XPS) was carried out using the Thermo Scientific ESCALAB 250Xi spectrometer. Inductively coupled plasma mass spectrometry (ICP-MS) analyses were performed using a PerkinElmer Elan DRC II Quadrupole instrument. Fourier transform infrared spectra (FT-IR) were obtained on a SHIMADZU IRTracer-100 instrument. Cyclic voltammogram (CV) tests were conducted on a CHI 760 electrochemical workstation. Electrochemical impedance spectroscopy (EIS) were recorded on a Metrohm Autolab electro-workstation.

Synthesis of Conjugated Microporous Polymer (CMP). Carbon cloths (CCs) were first cut into 1 cm × 1.5 cm small pieces as electrode substrates, ultrasonically cleaned in ethanol and acetone for 30 min each, and then dried in a vacuum oven at 80 °C. A mixture of acetonitrile (CH_3CN, 10.0 mL) and dichloromethane (CH_2Cl_2, 30.0 mL) was used as an electrolyte solution. Then, 4,4′,4″-tris(carbazol-9-yl)-triphenylamine (TCTA, 0.1 mmol), N-(2-cyanoethyl)-pyrrole (NCP, 0.1 mmol), and tetrabutylammonium hexafluorophosphate (Bu_4NPF_6, 0.1 M) were added into the above electrolyte solution and then stirred to form a homogeneous solution. Electropolymerization of CMP over CC electrodes was carried out in a standard three-electrode cell with a nonaqueous Ag/Ag^+ (0.01 M) as the reference electrode, a platinum sheet as the counter electrode, and treated CC as the working electrode. CV measurements were performed in the standard three-electrode system with CMP growth in the voltage range of −0.5 to 1.5 V at a scan rate of 10 mV/s, and CMP-coated electrodes were obtained after 20 cycles. CMP-AO was synthesized by amidoximation of a nitrile (−CN) containing polymer using a mixture of hydroxylamine hydrochloride ($NH_2OH{\cdot}HCl$, 250.0 mg) and triethylamine (TEA, 0.6 mL) in anhydrous ethanol (10.0 mL) for 24 h before being washed with ethanol to obtain CMP-AO electrodes. The AO density of CMP-AO was determined using the equation in the Supporting Information.

Uranium Extraction Studies. For the physicochemical adsorption, in order to study the physicochemical adsorption properties, the CMP-AO electrode was immersed in the uranyl spiked solution, and the uranium concentration in the solution was analyzed at specific time intervals to study the adsorption kinetics. The isotherm experiments were then carried out on aqueous solutions spiked with uranyl at an initial concentration of 10−200 ppm.

For the electrochemical extraction of U(VI), all electrochemical uranium extraction tests were carried out in a two-electrode system with a graphite rod as the anode and a self-supporting CMP-AO electrode as the cathode. A series of U(VI) electrochemical extraction experiments as a function of pH, contact time, varying U(VI) concentration, and competing/selectivity ions were conducted at room temperature. In a typical experiment, the electrode loaded CMP-AO (2−4 mg) was placed into 20 mL of U(VI) solution (10−200 mg/L) in a electrochemical cell. The solution pH values were adjusted between 3.0 and 9.0 by adding negligible volumes of 0.1 M HCl or NaOH. Under the asymmetrical alternating current electrochemistry (AACE) method (RIGOL, DG1022A), the working voltages were alternating from −5 to 0 V with durations of 1 and 1.5 ms, respectively. After magnetic stirring for ∼6 h, the concentrations of U(VI) in the aqueous solution were analyzed by SP−721E using the Arsenazo III spectrophotometric method at a wavelength of 650 nm. In the physicochemical adsorption case, U(VI) adsorption kinetics and isotherm studies were carried out by the aforementioned procedure without the aid of an extra AACE.

https://doi.org/10.1021/cbe.4c00141
Chem Bio Eng. 2025, 2, 53−63

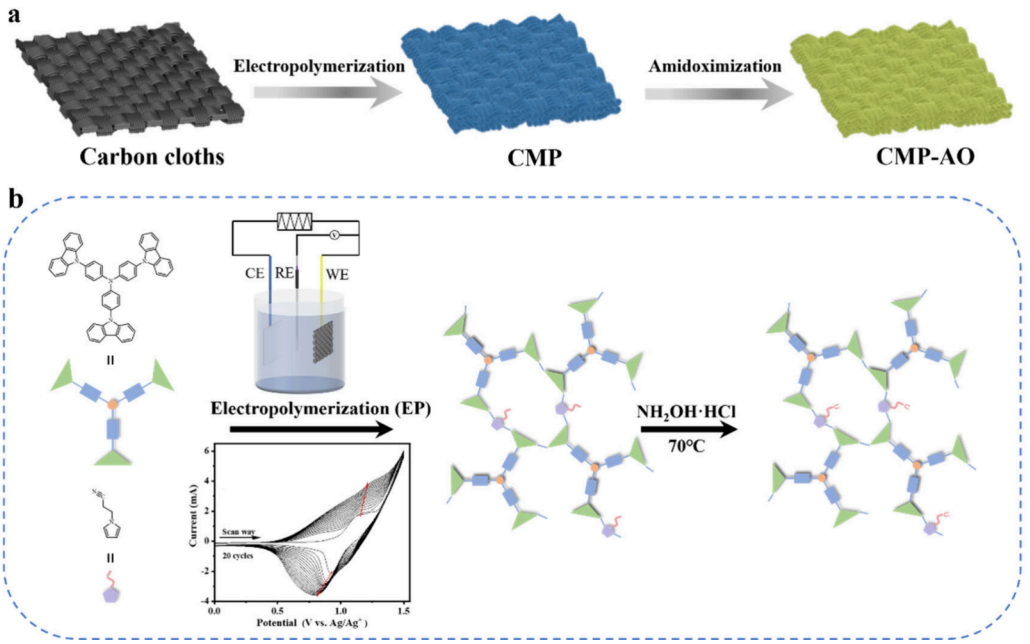

Figure 1. (a) Schematic diagrams of the preparation of CMP-AO electrode. (b) CV profiles and molecule structures of monomers (TCTA and NCP), CMP, and CMP-AO.

The influence of interfering ions (20 mL each of Na^+, K^+, Mg^{2+}, Ca^{2+}, Cu^{2+}, Co^{2+}, Sr^{2+}, Ba^{2+}, Pb^{2+}, and VO_3^-) on electrochemical extraction of U(VI) were performed in identical concentration of U(VI)-spiked water. Furthermore, the selectivity of CMP-AO for U(VI) over various other relevant metal ions (10 ppm of Ni^{2+}, Zn^{2+}, Ba^{2+}, Sr^{2+}, and VO_3^-) was also conducted at T = 293 K with 6 h contact time. The concentrations of these cation ions in the supernatant were examined using ICP-MS. For the repeatability testing, the U(VI)-carrying electrode was treated by placing the sample in a mixture solution of 1.0 M Na_2CO_3 and 0.1 M H_2O_2 to elute the bound uranium. After this treatment, the electrode can be reused for the next electrochemical uranium removal cycle.

RESULTS AND DISCUSSION

Preparation and Characterization of CMP and CMP-AO Electrodes. The electrochemical polymerization (EP) derived CMP over CCs was prepared by using a conventional three-electrode device, as shown in Figure 1a. Through an electropolymerization strategy, CMP can be polymerized onto a textile CC substrate. Two electroactive monomers, 4,4′,4″-tris(carbazol-9-yl)-triphenylamine (TCTA) and N-(2-cyanoethyl)pyrrole (NCP), were taken as building blocks for the coconstruction of CMP, in which TCTA has three active carbazole blocks with a triphenylamine core,[19] whereas the carbazole groups can be polymerized under an electric field, and they can act as high-pressure redox active centers, resulting in the formation of three-dimensional microporous networks.[18,20] And the −CN groups in NCP could be modified with amidoxime groups using $NH_2OH{\cdot}HCl$, which has a strong binding affinity for uranyl through synergistic interactions. Thus, the amidoxime molecule can selectively adsorb UO_2^{2+} to the electrode surface, which is then catalytically converted to U(V) by the redox-active carbazole unit. Cyclic voltammetry (CV) is widely used to study the kinetics of electrochemical polymerization and the electrode processes of electrochemical polymerization. Thus, the EP process was performed using CV between the potential range of −0.5−1.5 V in the CH_2Cl_2/CH_3CN mixture (vs Ag/Ag^+) (Figure S1). The CV change curves of the whole electrochemical polymerization are also plotted in Figure 1b. In the anodic scan, two oxidation peaks appeared at 0.8 and 1.18 V due to the formation of pyrrole and carbazole radical cations, resulting in the coupling of these cationic radicals to produce dimers, which is susceptible to oxidation to cationic radicals (Figure S2).[21,22] During cathodic scanning, the dimerized cation was reduced to the neutral state by two one-electron steps, which resulted in two peaks at 1.03 and 0.88 V, respectively.[23] As EP proceeds, the peak shifts toward higher potentials accompanied by the increasing peak current after 20 cycles, implying the gradual growth of CMP on the CC substrate.[24−26] Upon completion of the electropolymerization, the CMP composite was placed with a freshly prepared hydroxylamine solution to complete the amidoximation (AO) reaction of nitrile-containing polymers (denoted as CMP-AO).

The corresponding morphologies of these samples (CCs, CMP, and CMP-AO) were characterized by SEM. SEM images of CCs and CMP revealed that the smooth CCs skeleton was homogeneously covered by 2D short fibrils arrays through the feasibility of the EP process for the growth of organic polymers on the electrically conductive base (Figure 2a and b). After amidoximation (Figure 2c), the fibrous morphology was still well-preserved, indicating the electropolymerized CMP had good stability. Clearly, the densely packed CMP-AO layer was conformally arranged on the surface after two-step reaction. To gain insight into the special structures, SEM EDS elemental mapping images revealed the change of element content for the as-synthesized samples (Figure 2d, Figure S3, and Table S1). Notably, the significant increasing N content for CMP and N/O content for CMP-AO demonstrated the successful introduction of conjugated polymers and amidoxime before and after the amidoximation process. The matched spatial distributions of C, N, and O further confirmed the homogeneous dispersion of copolymers on the CCs skeleton. After the EP process, the corresponding hydrophilicity of these material were measured, and the water contact angle slightly decreased from bare CCs (124.8°) to

https://doi.org/10.1021/cbe.4c00141
Chem Bio Eng. 2025, 2, 53−63

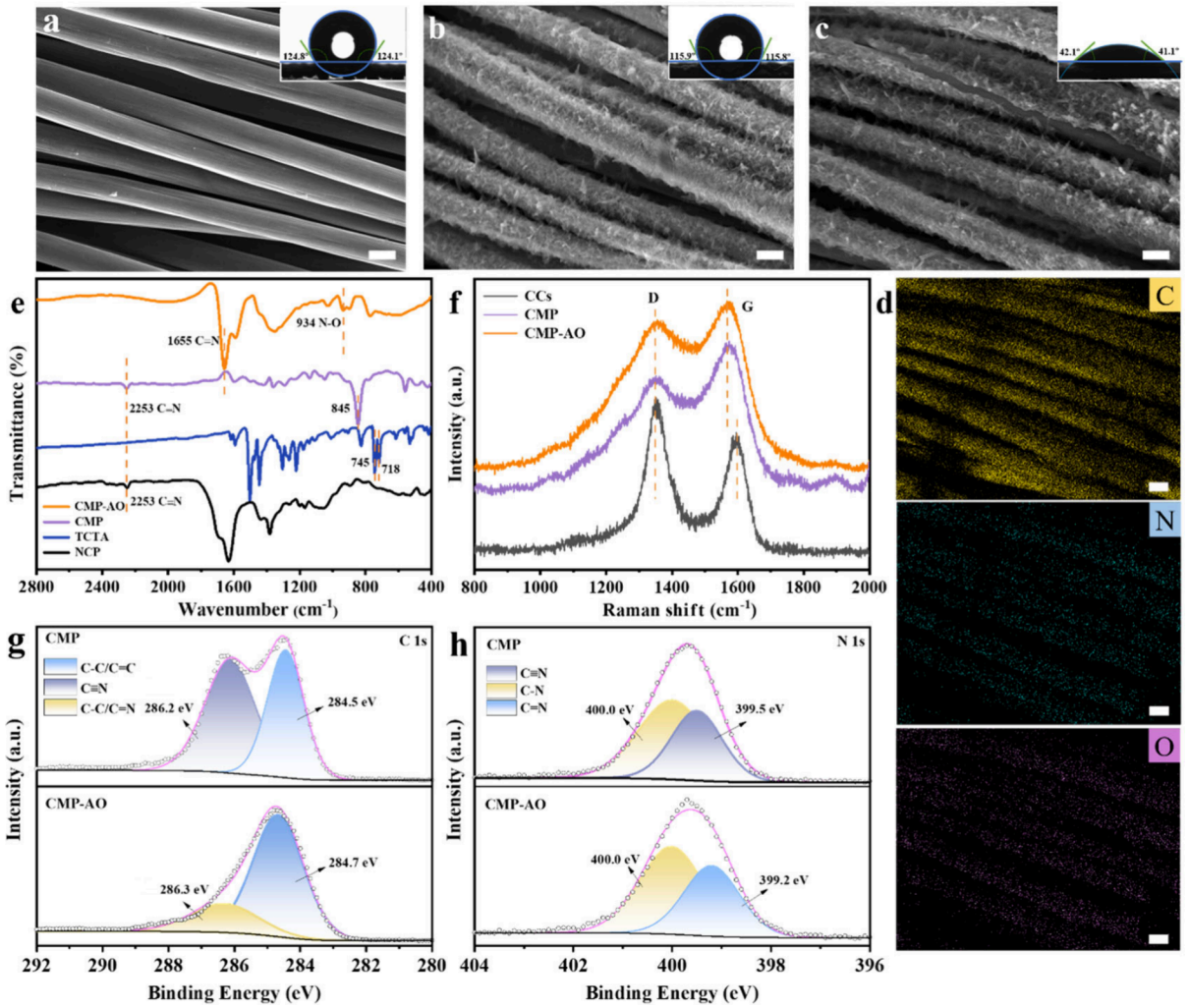

Figure 2. SEM images of CCs (a), CMP (b), and CMP-AO (c) (scale bar: 10 μm, and the insets are the corresponding contact angles for deionized water on these substrates). (d) EDS patterns of CMP-AO (scale bar: 10 μm). (e) FT-IR spectra of the TCTA monomer, NCP monomer, CMP, and CMP-AO samples. (f) Raman spectra of CCs, CMP, and CMP-AO. High-resolution spectra of C 1s (g) and N 1s (h) for CMP and CMP-AO, respectively.

CMP electrode (115.8°) (inset in Figure 2a and b). Excitingly, the contact angle of water droplets on the CMP-AO electrode (41.1°) was significantly weakened in comparison to the CMP one (115.8°) due to the excellent hydrophilicity of the amidoxime groups (inset in Figure 2c). The modified hydrophilicity of amidoximation in CMP-AO could facilitate the diffusion of U(VI) from the solution to the electrode surface, thereby augmenting U(VI) capture. Electrochemical impedance spectroscopy (EIS) was employed to investigate the electrical conductivity of these electrodes (Figure S4). Both bare CCs and CMP-AO showed similar semicircularity in the high frequency region, while expressing linearly in the low frequency region.[27] In EIS Nyquist plots, before and after EP process, the arc radius, did not show any significant change, indicating their smaller charge transfer resistance, and fast charge transfer kinetics.[28,29] Furthermore, the electrochemical behavior of CMP-AO was investigated by CV, and the CMP-AO electrode exhibited two characteristic peaks at 0.393 and 0.174 V corresponding to the oxidation and reduction processes of ferricyanide (Figure S5), respectively, revealing that the EP derived material has good electrochemical activity.

The functional groups of precursors (TCTA and NCP), CMP, and CMP-AO were carefully examined to gain insight into the microstructures. In Fourier transform infrared (FT-IR) spectrum of TCTA, two vibration bands at ~745 and ~718 cm^{-1} were observed, which were indexed to the disubstituted benzene ring in benzene and carbazole, respectively (Figure 2e).[19,28] While the NCP monomer showed a sharp and medium intensity absorption band at 2253 cm^{-1}, which was assigned to the characteristic C≡N stretching peak.[30] The FT-IR spectrum of CMP revealed that the weakened disubstituted benzene ring accompanied by the new peak appeared at 845 cm^{-1} can be assigned to the trisubstituted benzene ring, suggesting the formation of conjugated polymers.[20,31] For comparison, the characteristic stretching band of the C≡N group completely disappeared in CMP-AO, and the appearance of C═N at 1655 cm^{-1} and N−O at 934 cm^{-1} verified the successful conversion of the cyano groups into the amidoxime groups. Subsequent Raman spectra further revealed the change in I_D/I_G, as an indication of the degree of edge roughness and structural defects of carbon-based materials (Figure 2f). Compared with the I_D/I_G value of pure CCs (~1.29), the values gradually decreased to ~0.85

https://doi.org/10.1021/cbe.4c00141
Chem Bio Eng. 2025, 2, 53−63

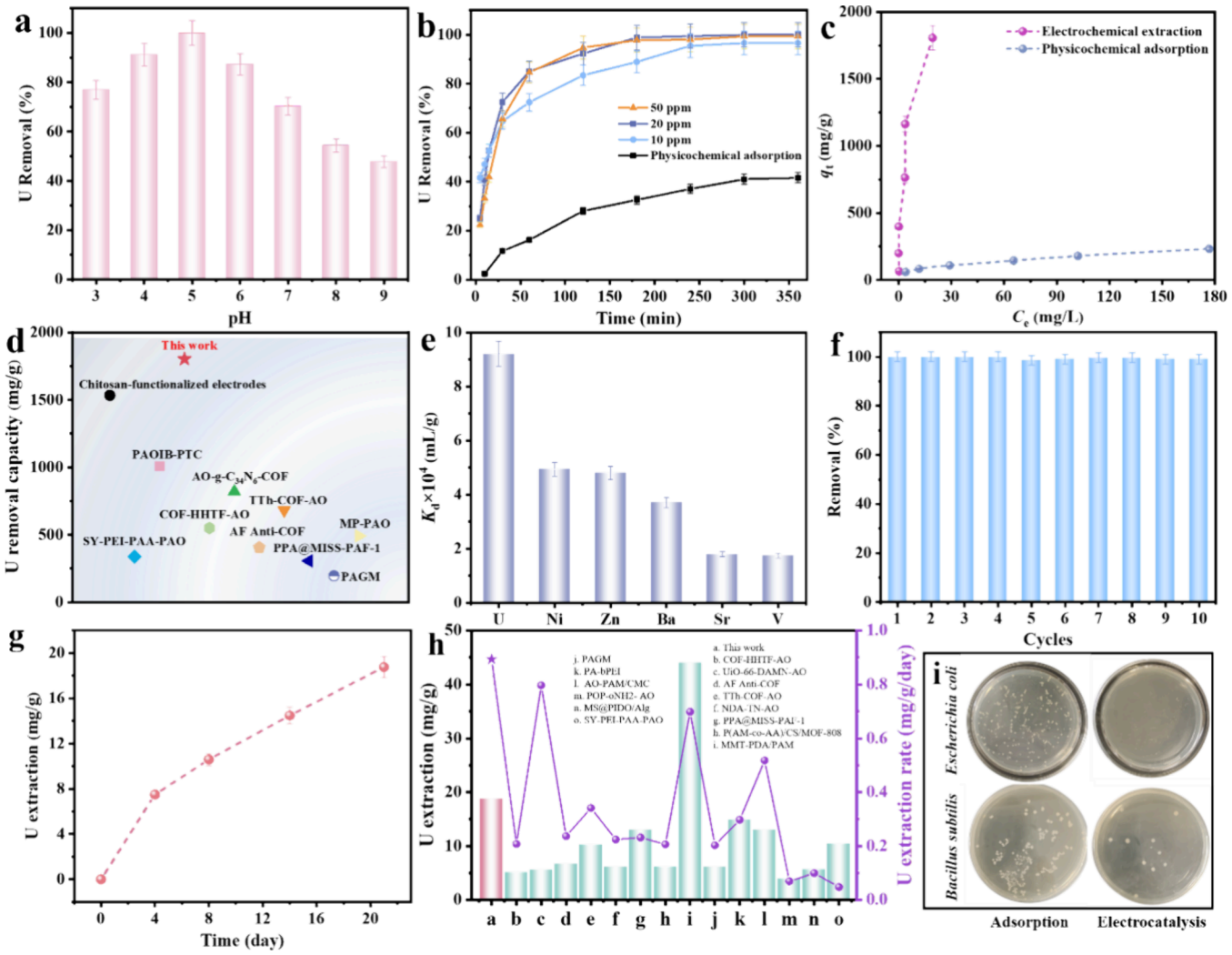

Figure 3. (a) Effect of varying pH from 3.0 to 9.0 on U(VI) extraction efficiency of CMP-AO. (b) Electrochemical extraction kinetics and physicochemical adsorption kinetics on CMP-AO. (c) Effect of initial concentration on U(VI) removal by electrochemical extraction and physicochemical adsorption. (d) Comparison of extraction capacities compared to other materials. (e) Selectivity coefficients of CMP-AO for U(VI) against various interfering ions. (f) Recyclability of CMP-AO for uranium extraction. All batch experiments were conducted in simulated solution ($C_{U(VI)}$ = 10−200 ppm, m/V = 0.1 g/L, t = 360 min, T = 293 K). (g) Uranium extraction capacities of CMP-AO electrode during 21 days of contact with real natural seawater in device-level continuous flow test. (h) Comparison of uranium extraction uptake performance of CMP-AO and other reported materials in natural seawater. (i) Photographs of *Escherichia coli* and *Bacillus subtilis* after treatment with CMP-AO without applying electric filed and under AACE conditions.

and ∼0.93 for CMP and CMP-AO, respectively. This phenomenon was due to the increased sp^2 hybridization carbon of CMP, which could effectively interact with the CCs substrate, supported by the CMP structure.

The atom states and coordination of these conjugated polymers were further confirmed by X-ray photoelectron spectroscopy (XPS). XPS survey spectra in Figure S6 showed remarkable enhanced O signals in CMP-AO compared to CMP. As can be seen in Figure 2g, the high-resolution C 1s spectrum of CMP can be divided into C−C/C═C at 284.5 eV and C≡N at 286.2 eV, respectively.[32,33] After amidoxime functionalization, both binding energy peaks appeared at 284.7 and 286.3 eV in CMP-AO, representing C−C/C═C and C−N/C═N, respectively.[34,35] Predictably, the N 1s spectrum of CMP had two signal at 400.0 and 399.5 eV,[36] corresponding to C−N and C≡N, while the N environments of CMP-AO was deconvoluted into two distinct peaks at 400.0 and 399.2 eV, which were identified as C−N and C═N in the carbazole units and amidoxime groups, respectively (Figure 2h).[37−39]

AACE for Uranium Extraction. The electrochemical performance of CMP-AO in uranium extraction was systematically investigated using the AACE method with potentials ranges from −5 to 0 V at a frequency of 400 Hz. The electrochemical characteristics of uranium were investigated in uranyl-spiked seawater and natural seawater through the CV method (Figure S7). There was no obvious reduction/oxidation peak in the natural seawater. The CV curves of uranyl-spiked seawater revealed a distinct peak at −0.46 V (vs SCE) which can be assigned for the reduction of U(VI) to U(V), and a peak at −0.03 V (vs SCE) as a result of the oxidation of U(V) to U(VI).[11,16,40] Similarly, a distinct redox peak appeared in the CV curve of the uranyl-spiked ultrapure water. The U(VI) extraction performance of these flexible electrode materials (CCs, PTCTA, PNCP-AO, CMP, and CMP-AO) was tested (Figure S8). Compared with the pure

https://doi.org/10.1021/cbe.4c00141
Chem Bio Eng. 2025, 2, 53−63

CCs, the electropolymerized materials synthesized under identical conditions showed remarkable enhanced U(VI) removal capacities. Due to the microporous network and the abundant functional amidoxime/carbazole groups, CMP-AO achieved outstanding removal capacity relative to other electropolymerized materials. Meanwhile, the effect of applying different negative voltages on the electrosorption of U(VI) was investigated (Figure S9). One can see that the extraction efficiency of U(VI) gradually increased with the increasing applied negative voltage, and the extraction efficiency of U(VI) reached nearly 100% at −5 and 0 V. Therefore, the CMP-AO electrode was taken as an example to evaluate the ability for U(VI) extraction by adopting the operation voltage that alternated between −5 and 0 V.

The pH of the aqueous solution can determine the U(VI) species (Figure S10). A series of AACE experiments were further carried out by controlling pH as a single variable in the range of pH = 3.0−9.0. As shown in Figure 3a, the removal rates of U(VI) over CMP-AO was increased with increasing pH from 3.0 to 5.0, followed by a subsequent decline at pH > 5.0. This optimal pH analysis was well agreement with previous containing amidoxime group-based materials.[3,17]

Time-dependent physicochemical adsorption process displayed that ∼41.6% U(VI) was adsorbed on CMP-AO within 6 h at an initial U(VI) concentration of 20 ppm. In order to study the electrosorption-catalysis kinetics, the U(VI) extraction kinetics were carried out in U(VI)−spiked aqueous solution with three different U(VI) concentrations of 10, 20, and 50 ppm, respectively (Figure 3b). Interestingly, the AACE process exhibited a fast response within the initial contact of 1 h and gradually reached equilibrium at 3 h. The final removal efficiencies of all three initial U(VI) concentrations over CMP-AO were up to ∼100%. When bias was added, the physicochemical adsorption−desorption equilibria would be broken, and the electro field could promote the mass transfer diffusion of U(VI) on the CMP-AO surface. The presence of amidoxime groups and carbazole units in the CMP-AO network provided the effective binding sites and catalytic sites, which synergistically promoted the electrosorption-catalysis process. Clearly, Figure S11 presented the AACE process of CMP-AO toward U(VI) at high initial concentration (∼500 ppm) as a function of reaction time at room temperature. It was found that the electrochemical system provided powerful electrically driving force to the U(VI) ions directed diffusion from the solution to CMP-AO surface, resulting in the pale-yellow floc wrapped the CMP-AO electrode. In addition, the AACE process was simulated using pseudo-first-order kinetic (Figure S12 and Table S2). The results of correlation coefficient (R^2) fitting for 10, 20, and 50 ppm were 0.965, 0.965, and 0.975, respectively. The physicochemical adsorption kinetics were fitted by pseudo-first-order and pseudo-second-order models, respectively (Figure S13 and Table S3). The pseudo-second-order kinetics model was preferable for describing physicochemical adsorption kinetics (R^2 > 0.98), indicating that chemisorption dominated the adsorption process because of the coordination between the functional groups on the surface and target ions. Correspondingly, the comparative isotherms of U(VI) extraction on CMP-AO were investigated under physicochemical and AACE methods. For the physicochemical adsorption, the maximum adsorption capacity (q_{max}) of CMP-AO toward U(VI) was calculated to be ∼245.30 mg/g (Figure S14 and Table S4). And the equilibrium adsorption data were well described by a Freundlich model, giving rise to a high R^2 equal to 0.99. For AACE extraction, the q_e could attain as high as ∼1806.4 mg/g in 200 ppm of U(VI) simulated solution, which did not seem to reach the saturation. The U(VI) extraction performance of CMP-AO exhibited an ultrahigh uranium removal capacity compared to most reported materials via different methods (Figure 3d and Table S5). This self-standing CMP-AO electrode material would be a promising high-efficient capturer for massive uranium extraction from seawater.

As uranyl in solution generally exists in a complex ionic coexistence environment, various interfering ions may compete with uranyl ions for binding sites on the surface of CMP-AO. One can see that a negligible effect of these various individual foreign ions on U(VI) AACE extraction onto CMP-AO was observed (Figure S15). In particular, the AACE extraction selectivity in the coexistence of different competing metal ions (V^{5+}, Ba^{2+}, Ni^{2+}, Sr^{2+}, etc.) was also studied (Figure 3e). The distribution coefficient (K_d) is used for the determination of the affinity and selectivity of materials for U(VI). In general, the materials with K_d values >10^4 mL/g are recognized as good adsorbents.[41] Impressively, the K_d^U of CMP-AO demonstrated a high value K_d^U of approximately ∼9.63 × 10^4 mL/g, which preferred U(VI) over other competitive metal ions. The unique structure of CMP-AO stemmed from its amidoxime chelating groups selective for U(VI) target ions. When the pulsed voltage was applied, the CMP-AO electrode could capture target ions and repel unbound ions during the electrochemical process aided in the extraction of uranium.

To assess the reusability and stability of CMP-AO, the uranium-laden CMP-AO could readily be regenerated by treatment with a mixed solution of 0.1 M Na_2CO_3 and 0.1 M H_2O_2. As shown in Figure 3f, no obvious change of the removal efficiency was observed after ten successive electrochemical adsorption/desorption cycles. The CMP-AO layer was still firmly wrapped on the skeleton of CCs substrate, demonstrating that CMP-AO showed a good reusability and could serve as a good capturer in the field of U(VI) removal and recovery. In addition, we investigated the FT-IR spectra of CMP-AO loaded with uranium and the eluted one (Figure S16). No structural damage was observed to the FT-IR spectra of CMP-AO after the test. The characteristic antisymmetric vibration peak of the O═U═O can be clearly observed at 900 cm^{-1} in the uranium-loaded spectrum. However, after elution, the O═U═O peak disappeared, and N−OH recovered at 934 cm^{-1}, indicating the recovery of amidoxime-functionalized CMP-AO. Based on the results of the above experiments, we tested the adsorption-electrochemical uranium extraction performance of CMP-AO in uncalibrated natural seawater (with an approximate uranium concentration of ∼3.3 ppb), and a homemade flow device is shown in Figure S17. As shown in Figure 3g, the extraction capacity of uranium was almost linearly related to the reaction time, reaching a high extraction capacity of 7.50 mg/g in 4 days. After the electrochemical system was durably operated in natural seawater for 21 days, an excellent extraction performance of 18.8 mg/g was achieved. Meanwhile, the extraction rate of uranium over CMP-AO was up to ∼0.90 mg/g/day, which was greater than that of the vast majority of previously reported materials (Figure 3h and Table S5). Thus, deploying a CMP-AO electrode in an adsorption-electrocatalysis system can provide a potential fast and high uranium extraction method from seawater.

https://doi.org/10.1021/cbe.4c00141
Chem Bio Eng. 2025, 2, 53−63

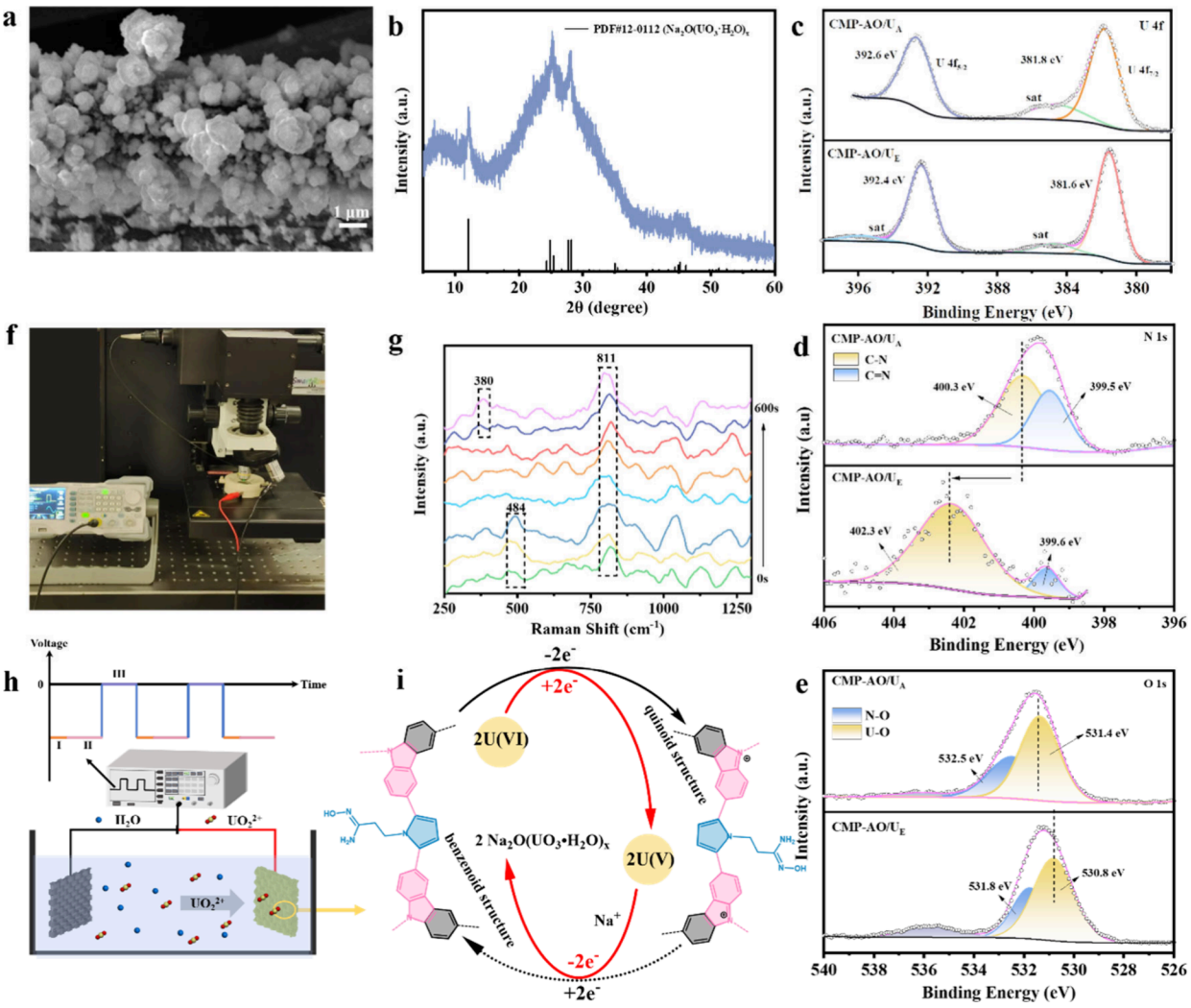

Figure 4. SEM image (a) and PXRD pattern (b) of the yellow precipitation. (c) U 4f XPS spectra of CMP-AO after physicochemical adsorption and electrocatalysis. The high-resolution XPS spectra of N 1s (d) and O 1s (e) for CMP-AO/U_E and CMP-AO/U_A, respectively. (f) Photo of the full setup. (g) In situ Raman spectra collected from the CMP-AO working electrode in uranium solution during the adsorption-electrocatalysis process. (h) Schematics of the AACE extraction process and (i) rational reaction mechanism for uranium extraction with the CMP-AO electrode.

Antibiofouling Studies. Because of the complexity of natural seawater system, marine microorganisms may affect the extraction performance of CMP-AO electrode for uranium capture. The antibacterial activities of CMP-AO in adsorption and electrocatalysis systems were studied by the spread plate method, and the colonies on agar are shown in Figure 3i. The inhibition rates of *Escherichia coli* and *Bacillus subtilis* were ~81% and ~98% for CMP-AO in the electrocatalysis system, which were considerably superior to the inhibition rates in the physicochemical adsorption system. With the aid of an extra AACE, the redox homeostasis across the cell membrane would be disrupted by the electric filed, which would lead to excessive reactive oxygen species.[42,43] The resulting reactive oxygen species could lead to lipid peroxidation of cell membrane and distorts biomolecules, further inhibiting growth of marine bacteria.[44] The inhibition effect of AACE operation on bacterial growth demonstrated that CMP-AO electrode in adsorption-electrocatalysis system could synchronously realize the uranium extraction and potent antibiofouling properties.

Uranium Extraction Mechanism. The combined electrochemical analyses and spectroscopic characterizations were employed to investigate the electrochemical extraction mechanism of uranium by CMP-AO. From the CV scan curves of natural seawater and uranyl-spiked seawater (~10 and 200 ppm at pH = 8.1), uranyl-spiked seawater showed a peak at −0.46 V (vs SCE), which represents the reduction of U(VI) to U(V), and U(V) would conduct an oxidation reaction into U(VI) at −0.03 V (versus SCE),[11,16,40] but there was no corresponding peak in natural seawater. Thus, CMP-AO is capable of reducing U(VI). The SEM images at different magnifications of CMP-AO electrode after U(VI) extraction was characterized to gain insight into the morphology change (Figure S18). It was discovered that a large amount of micrometer-sized particles was attached to the CMP-AO electrode surface. A high magnification SEM image indicated that the morphology resembled bunches of grapes with diameters of 0.2−1.0 μm (Figure 4a). Accordingly, the resulting micron-sized particles on the electrode were identified as $Na_2O(UO_3{\cdot}H_2O)_x$ (PDF#12−0112) via PXRD characterization (Figure 4b), which is consistent with previous studies.[11,45,46] Note that the characteristic U(VI) signal in the uranium-loaded CMP-AO was significantly red-shifted from ~963 cm^{-1} (the aqueous UO_2^{2+} complexes) to 900 cm^{-1} in the FT-IR spectra (Figure S16),[47] suggesting a strong

https://doi.org/10.1021/cbe.4c00141
Chem Bio Eng. 2025, 2, 53−63

interaction between uranium and the active sites in CMP-AO network.

XPS was applied to further probe the interaction between CMP-AO and uranium species. From the XPS survey spectra of CMP-AO, CMP-AO after physicochemical adsorption (denoted as CMP-AO/U_A), and CMP-AO after electrochemical extraction (denoted as CMP-AO/U_E), all three samples showed the predominant elements of O 1s, N 1s and C 1s, respectively (Figure S19). Notably, the Na 1s signal that emerged in the XPS survey spectra of CMP-AO/U_E was significantly higher than that of CMP-AO/U_A, indicating the formation of sodium compounds in the product. However, sharp peaks of U 4f emerged in the XPS spectra of CMP-AO/U_A and CMP-AO/U_E (not present in the XPS spectrum of CMP-AO). From Figure 4c, the high-resolution XPS spectrum of U 4f in CMP-AO/U_A could be divided into two prominent peaks 381.8 and 392.6 eV, which were ascribed to U $4f_{7/2}$ and U $4f_{5/2}$, respectively.[48] In contrast, the above two peaks in CMP-AO/U_E were located at 381.6 and 392.4 eV, signifying a 0.2 eV shift compared to that of CMP-AO/U_A. Compared with CMP-AO/U_A, the C−N/C═N bond in C 1s XPS spectra of CMP-AO/U_E was distinctly observed to shift toward relatively higher binding energy from 286.9 to 288.5 eV, suggesting that the C−N/C═N was engaged in the uranium extraction (Figure S20). Moreover, after physicochemical adsorption, the two peaks (C−N and C═N) were both found to be slightly shifted to 400.3 and 399.5 eV in the N 1s spectra of CMP-AO/U_A (Figure 4d). In the case of AACE, the C−N and C═N binding energies that significantly shifted to higher binding energies (402.3 and 399.6 eV) also demonstrated the strong interaction of amidoxime/carbazole groups and uranium species. By way of bonding with U(VI), the extranuclear electron density of N decreased due to the coordination of U(VI) with the amidoxime group, and the N-substituted carbazole units, as redox-active centers, provided the driving force to facilitate the electron transfer from the N atom to the absorbed uranyl ions in the electrocatalysis reaction. The different adsorption and electrochemical extraction approaches resulted in a varying degree of the binding energy shift.[34,49,50] Inversely, the binding energy of the N−O peak shifted to the lower side in O 1s spectra of CMP-AO/U_A and CMP-AO/U_E, and a new peak that emerged at 530.8 eV was assigned to the U−O bond in the O 1s spectra (Figure 4e).[51]

Furthermore, the nature of the electrochemical extraction process in the CMP-AO electrode was recorded using in situ Raman analysis. As shown in Figure 4f and g, after soaking CMP-AO electrode in uranium-spiked seawater for 30 min, the dominant band at 811 cm^{-1} can be assigned to the symmetric stretching of O═U═O, while the main spectral feature in the range of 100−500 cm^{-1} represented the bending vibrations of UO_2^{2+}, in which the Raman signal appeared at 484 cm^{-1}, originating from the adsorbed uranyl ions. As time progressed, the peak intensity of adsorbed uranyl ions gradually decreased and disappeared completely during the AACE extraction process. This phenomenon might be the conversion of adsorbed U(VI) to the U(V) intermediate. However, the U(V) lifetime was too short to monitor the reaction intermediate on the electrode surface to be observable by the optical techniques.[52] The emerging U(V) signal could be considerably demonstrated by CV analysis. As the AACE extraction time operated up to ∼600 s, a new peak at 380 cm^{-1} was detected on the CMP-AO electrode, suggesting the oxidation of unstable U(V) back to U(VI). The presence of Na^+ was beneficial to maintain the stability of uranium species and finally form the $Na_2O(UO_3{\cdot}H_2O)_x$ precipitate, which was consistent with the PXRD result. Taken together, the possible mechanism of uranium extraction from seawater by the integrating adsorption-electrocatalysis system was proposed (Figure 4h and i). (I) When a negative potential was applied, the discrete amidoxime group in the CMP-AO network could capture the U(VI) ions separately from seawater in which all ions were randomly dispersed. (II) Then, the adjacent carbazole units in CMP-AO would each lose an electron, leading to the transformation of the benzenoid structure to the quinoid structure (N^+-substituted carbazole). Meanwhile, by transferring a single electron to U(VI), U(VI) was reduced to U(V). Subsequently, the oxidation of U(V) to U(VI) transferred an electron back to the N^+-substituted carbazole site, thereby regenerating N-substituted carbazole. In addition, the coexisting Na^+ ions resulted in the $Na_2O(UO_3{\cdot}H_2O)_x$ precipitates. (III) When the bias was removed, other interfering ions that did not bind with CMP-AO would be released into the solution. Overall, such a reversible electron transfer process could facilitate the electrodeposition of uranium compounds on the electrode, consequently yielding a pale-yellow floc product.

CONCLUSIONS

In summary, an electropolymerized CMPs-AO adsorption-electrocatalyst was developed as a highly efficient uranium extraction material from seawater. The intriguing CMP-AO structure with good hydrophilicity, featuring surface-specific binding sites (amidoxime groups) and redox-active centers (N-substituted carbazole units), endowed the functionalized electrode with a high affinity for uranyl ions and subsequently provided an excellent reversible electron transfer platform for the eventual generation of $Na_2O(UO_3{\cdot}H_2O)_x$ products. Benefitting from the unique advantages of chemical adsorption and electrochemical reduction, the CMP-AO electrode in the adsorption-electrocatalysis system exhibited fast kinetics with short equilibrium time (<3 h), high extraction capacity without saturation (∼1806.4 mg/g), good selectivity with a distribution coefficient (K_d^U) value of approximately ∼9.63 × 10^4 mL/g against V^{5+}, Ba^{2+}, Ni^{2+}, and Sr^{2+}, and outstanding antibacterial activity (>81%). This work provides an appealing direction to in situ fabricate advanced conducting adsorption-electrocatalysts with metal free for electrochemical uranium extraction from natural seawater.

ASSOCIATED CONTENT

Supporting Information

The Supporting Information is available free of charge at https://pubs.acs.org/doi/10.1021/cbe.4c00141.

Chemicals, materials characterization methods, computational details, supplemental figures and tables (PDF)

AUTHOR INFORMATION

Corresponding Authors

Tao Wen − *MOE Key Laboratory of Resources and Environmental Systems Optimization, College of Environmental Science and Engineering, North China Electric Power University, Beijing 102206, P.R. China;* orcid.org/0000-0001-9089-3196; Phone: +86-10-61772890; Email: twen@ncepu.edu.cn

https://doi.org/10.1021/cbe.4c00141
Chem Bio Eng. 2025, 2, 53−63

Xiangke Wang − *MOE Key Laboratory of Resources and Environmental Systems Optimization, College of Environmental Science and Engineering, North China Electric Power University, Beijing 102206, P.R. China;* orcid.org/0000-0002-3352-1617; Email: xkwang@ncepu.edu.cn

Authors

Xinyue Zhang − *MOE Key Laboratory of Resources and Environmental Systems Optimization, College of Environmental Science and Engineering, North China Electric Power University, Beijing 102206, P.R. China*

Xinying Lei − *MOE Key Laboratory of Resources and Environmental Systems Optimization, College of Environmental Science and Engineering, North China Electric Power University, Beijing 102206, P.R. China*

Hongfei Sun − *MOE Key Laboratory of Resources and Environmental Systems Optimization, College of Environmental Science and Engineering, North China Electric Power University, Beijing 102206, P.R. China*

Hanming Ke − *MOE Key Laboratory of Resources and Environmental Systems Optimization, College of Environmental Science and Engineering, North China Electric Power University, Beijing 102206, P.R. China*

Jingxuan Xu − *MOE Key Laboratory of Resources and Environmental Systems Optimization, College of Environmental Science and Engineering, North China Electric Power University, Beijing 102206, P.R. China*

Yuhao Yang − *MOE Key Laboratory of Resources and Environmental Systems Optimization, College of Environmental Science and Engineering, North China Electric Power University, Beijing 102206, P.R. China*

Sai Zhang − *Beijing Key Laboratory of Environmental and Viral Oncology, College of Chemistry and Life Science, Beijing University of Technology, Beijing 100124, China*

Zhuoyu Ji − *MOE Key Laboratory of Resources and Environmental Systems Optimization, College of Environmental Science and Engineering, North China Electric Power University, Beijing 102206, P.R. China;* orcid.org/0000-0002-8319-7093

Complete contact information is available at: https://pubs.acs.org/10.1021/cbe.4c00141

Author Contributions

X.Y.Z., T.W., and X.K.W. designed the overall project. X.Y.Z. and T.W.: Experiments, Writing−original draft, Review & editing. X.Y.Z.: Investigation, Experiments, Writing−original draft. X.Y.L.: Experimental method. H.F.S., H.M.K., and J.X.X.: Investigation. Y.H.Y.: Assistance of antimicrobial experiments. S.Z. and Z.Y.J.: Characterization analysis. X.K.W.: Supervision, Funding acquisition, Project administration, Review & editing.

Notes

The authors declare no competing financial interest.

■ ACKNOWLEDGMENTS

The authors gratefully acknowledge the National Natural Science Foundation of China (22476046; U23A20105), Science Challenge Project (No. TZ2016004), and Beijing Outstanding Young Scientist Program.

■ REFERENCES

(1) Kim, J.; Tsouris, C.; Mayes, R. T.; Oyola, Y.; Saito, T.; Janke, C. J.; Dai, S.; Schneider, E.; Sachde, D. Recovery of Uranium from Seawater: A Review of Current Status and Future Research Needs. *Sep. Sci. Technol.* **2013**, *48* (3), 367−387.

(2) Abney, C. W.; Mayes, R. T.; Saito, T.; Dai, S. Materials for the Recovery of Uranium from Seawater. *Chem. Rev.* **2017**, *117* (23), 13935−14013.

(3) Wang, Z.; Meng, Q.; Ma, R.; Wang, Z.; Yang, Y.; Sha, H.; Ma, X.; Ruan, X.; Zou, X.; Yuan, Y.; Zhu, G. Constructing An Ion Pathway for Uranium Extraction from Seawater. *Chem.* **2020**, *6* (7), 1683−1691.

(4) Wang, D.; Song, J.; Wen, J.; Yuan, Y.; Liu, Z.; Lin, S.; Wang, H.; Wang, H.; Zhao, S.; Zhao, X.; Fang, M.; Lei, M.; Li, B.; Wang, N.; Wang, X.; Wu, H. Significantly Enhanced Uranium Extraction from Seawater with Mass Produced Fully Amidoximated Nanofiber Adsorbent. *Adv. Energy Mater.* **2018**, *8* (33), No. 1802607.

(5) Cui, W. R.; Zhang, C. R.; Jiang, W.; Li, F. F.; Liang, R. P.; Liu, J.; Qiu, J. D. Regenerable and Stable Sp^2 Carbon-Conjugated Covalent Organic Frameworks for Selective Detection and Extraction of Uranium. *Nat. Commun.* **2020**, *11* (1), 436.

(6) Zhang, H.; Liu, W.; Li, A.; Zhang, D.; Li, X.; Zhai, F.; Chen, L.; Chen, L.; Wang, Y.; Wang, S. Three Mechanisms in One Material: Uranium Capture by a Polyoxometalate−Organic Framework through Combined Complexation, Chemical Reduction, and Photocatalytic Reduction. *Angew. Chem., Int. Ed.* **2019**, *58* (45), 16110−16114.

(7) Ling, L.; Zhang, W. X. Enrichment and Encapsulation of Uranium with Iron Nanoparticle. *J. Am. Chem. Soc.* **2015**, *137* (8), 2788−2791.

(8) Chen, Z.; Wang, J.; Hao, M.; Xie, Y.; Liu, X.; Yang, H.; Waterhouse, G. I. N.; Wang, X.; Ma, S. Tuning Excited State Electronic Structure and Charge Transport in Covalent Organic Frameworks for Enhanced Photocatalytic Performance. *Nat. Commun.* **2023**, *14* (1), 1106.

(9) Xie, Y.; Yu, L.; Chen, L.; Che, C.; Wang, L.; Liu, F.; Liao, Y.; Zhang, P.; Chen, T.; Yuan, Y.; Lu, Y.; Huang, B.; Yang, H.; Wang, S.; Wang, S.; Ma, L.; Luo, F.; Liu, Y.; Hu, B.; Wang, H.; Pan, D.; Zhu, W.; Wang, N.; Wang, Z.; Mao, L.; Ma, S.; Wang, X. Recent Progresses of Radionuclides Separation by Porous Nanomaterials. *Sci. China Chem.* **2024**, DOI: 10.1007/s11426-024-2218-8.

(10) Gao, P.; Hu, Y.; Shen, Z.; Zhao, G.; Cai, R.; Chu, F.; Ji, Z.; Wang, X.; Huang, X. Ultra-Highly Efficient Enrichment of Uranium from Seawater Via Studtite Nanodots Growth-Elution Cycle. *Nat. Commun.* **2024**, *15* (1), 6700.

(11) Yang, H.; Liu, X.; Hao, M.; Xie, Y.; Wang, X.; Tian, H.; Waterhouse, G. I. N.; Kruger, P. E.; Telfer, S. G.; Ma, S. Functionalized Iron−Nitrogen−Carbon Electrocatalyst Provides A Reversible Electron Transfer Platform for Efficient Uranium Extraction from Seawater. *Adv. Mater.* **2021**, *33* (51), No. 2106621.

(12) Wang, Z.; Ma, R.; Meng, Q.; Yang, Y.; Ma, X.; Ruan, X.; Yuan, Y.; Zhu, G. Constructing Uranyl-Specific Nanofluidic Channels for Unipolar Ionic Transport to Realize Ultrafast Uranium Extraction. *J. Am. Chem. Soc.* **2021**, *143* (36), 14523−14529.

(13) Liu, X.; Xie, Y.; Hao, M.; Li, Y.; Chen, Z.; Yang, H.; Waterhouse, G. I. N.; Wang, X.; Ma, S. Secondary Metal Ion-Induced Electrochemical Reduction of U(VII) to U(IV) Solids. *Nat. Commun.* **2024**, *15* (1), 7736.

(14) Liu, S.; Wang, Z.; Lu, Y.; Li, H.; Chen, X.; Wei, G.; Wu, T.; Maguire, D. J.; Ye, G.; Chen, J. Sunlight-Induced Uranium Extraction with Triazine-Based Carbon Nitride as Both Photocatalyst and Adsorbent. *Appl. Catal., B* **2021**, *282*, No. 119523.

(15) Hao, M.; Xie, Y.; Liu, X.; Chen, Z.; Yang, H.; Waterhouse, G. I. N.; Ma, S.; Wang, X. Modulating Uranium Extraction Performance of Multivariate Covalent Organic Frameworks through Donor−Acceptor Linkers and Amidoxime Nanotraps. *JACS Au* **2023**, *3* (1), 239−251.

(16) Liu, C.; Hsu, P. C.; Xie, J.; Zhao, J.; Wu, T.; Wang, H.; Liu, W.; Zhang, J.; Chu, S.; Cui, Y. A Half-Wave Rectified Alternating Current Electrochemical Method for Uranium Extraction from Seawater. *Nat. Energy* **2017**, *2* (4), No. 17007.

(17) Chen, D.; Li, Y.; Zhao, X.; Shi, M.; Shi, X.; Zhao, R.; Zhu, G. Self-Standing Porous Aromatic Framework Electrodes for Efficient Electrochemical Uranium Extraction. *ACS Cent. Sci.* **2023**, *9* (12), 2326−2332.

(18) Zhao, C.; Chen, Z.; Wang, W.; Xiong, P.; Li, B.; Li, M.; Yang, J.; Xu, Y. In-Situ Electropolymerization Enables Ultrafast Long Cycle Life and High-Voltage Organic Cathodes for Lithium Batteries. *Angew. Chem., Int. Ed.* **2020**, *59* (29), 11992−11998.
(19) Liang, Y.; Liu, C.; Zhao, M.; Wang, R.; Zhang, D.; Wang, C.; Zhou, L.; Wang, L.; Xie, Z.; Peng, J.; Liu, L. Organic Electropolymerized Multilayers for Light-Emitting Diodes and Displays. *ACS Appl. Mater. Interfaces* **2020**, *12* (18), 20714−20721.
(20) Gu, C.; Chen, Y.; Zhang, Z.; Xue, S.; Sun, S.; Zhang, K.; Zhong, C.; Zhang, H.; Pan, Y.; Lv, Y.; Yang, Y.; Li, F.; Zhang, S.; Huang, F.; Ma, Y. Electrochemical Route to Fabricate Film-Like Conjugated Microporous Polymers and Application for Organic Electronics. *Adv. Mater.* **2013**, *25* (25), 3443−3448.
(21) Ambrose, J. F.; Carpenter, L. L.; Nelson, R. F. Electrochemical and Spectroscopic Properties of Cation Radicals: III. Reaction Pathways of Carbazolium Radical Ions. *J. Electrochem. Soc.* **1975**, *122* (7), 876.
(22) Mangione, M. I.; Spanevello, R. A.; Minudri, D.; Heredia, D.; Fernandez, L.; Otero, L.; Fungo, F. Electropolimerization of Functionalizaed Carbazole End-Capped Dendrimers. Formation of Conductive Films. *Electrochim. Acta* **2016**, *207*, 143−151.
(23) Macit, H.; Sen, S.; Saçak, M. Electrochemical Synthesis and Characterization of Polycarbazole. *J. Appl. Polym. Sci.* **2005**, *96* (3), 894−898.
(24) Deng, Z.; Stone, D. C.; Thompson, M. Poly N-(2-Cyanoethyl)Pyrrole as a Selective Film for the Thickness-Shear-Mode Acoustic Wave Sensor. *Can. J. Chem.* **1995**, *73* (9), 1427−1435.
(25) Natera, J.; Otero, L.; Sereno, L.; Fungo, F.; Wang, N. S.; Tsai, Y. M.; Hwu, T. Y.; Wong, K. T. A Novel Electrochromic Polymer Synthesized through Electropolymerization of A New Donor−Acceptor Bipolar System. *Macromolecules* **2007**, *40* (13), 4456−4463.
(26) Wong, K. T.; Lin, Y. H.; Wu, H. H.; Fungo, F. Synthesis and Properties of Dumbbell-Shaped Dendrimers Containing 9-Phenylcarbazole Dendrons. *Org. Lett.* **2007**, *9* (22), 4531−4534.
(27) Wang, S.; Zhang, J.; Gharbi, O.; Vivier, V.; Gao, M.; Orazem, M. E. Electrochemical Impedance Spectroscopy. *Nat. Rev. Methods Primers* **2021**, *1* (1), 41.
(28) Zhang, H.; Zhang, Y.; Gu, C.; Ma, Y. Electropolymerized Conjugated Microporous Poly(Zinc-Porphyrin) Films as Potential Electrode Materials in Supercapacitors. *Adv. Energy Mater.* **2015**, *5* (10), No. 1402175.
(29) Shuang, M.; Zhou, L.; Liu, Y.; Yu, H.; Ao, X.; Ouyang, J.; Liu, Z.; Shehzad, H.; Adesina, A. A. Electrodeposition Nanofabrication of Graphene Oxide/Polypyrrole Electrodes with High Hybrid Specific Capacitance for Enhancing U(VI) Electrosorption. *J. Environ. Chem. Eng.* **2023**, *11* (6), No. 111498.
(30) Aradilla, D.; Estrany, F.; Armelin, E.; Oliver, R.; Iribarren, J. I.; Alemán, C. Characterization and Properties of Poly[N-(2-Cyanoethyl)Pyrrole]. *Macromol. Chem. Phys.* **2010**, *211* (15), 1663−1672.
(31) Sarac, A. S.; Sezer, E.; Ustamehmetoglu, B. Oxidative Polymerization of N-Substituted Carbazoles. *Polym. Adv. Technol.* **1997**, *8* (9), 556−562.
(32) Zhu, L.; Zhang, C.; Qin, F.; Ma, F.; Bi, C.; Zhu, R.; Liu, L.; Bai, J.; Dong, H.; Satoh, T. Amidoxime-Modified Hypercrosslinked Porous Poly(Styrene-Co-Acrylonitrile) Adsorbent with Tunable Porous Structure for Extracting Uranium Efficiently from Seawater. *J. Mol. Liq.* **2022**, *368*, No. 120741.
(33) Liu, X.; Ji, M.; Lin, H.; Jin, W.; Xue, Y.; Wang, Q.; Ma, F. Preparation of Amidoxime Polyacrylonitrile Membrane with Excellent Mechanical Strength for Adsorption of Uranium in Simulated Wastewater. *Sep. Purif. Technol.* **2023**, *327*, No. 124890.
(34) Tian, Y.; Wang, Y.; Liu, L.; Dong, H.; Zhu, X.; Ma, F.; Zhang, C. Fabrication of Amidoxime Functionalized Hyper-Cross-Linked Polymer for Efficient Extraction of Uranium (VI) from Water. *J. Mol. Liq.* **2023**, *372*, No. 121171.
(35) Xin, Q.; Wang, Q.; Luo, K.; Lei, Z.; Hu, E.; Wang, H.; Wang, H. Mechanism for the Seleikctive Adsorption of Uranium from Seawater Using Carboxymethyl-Enhanced Polysaccharide-Based Amidoxime Adsorbent. *Carbohydr. Polym.* **2024**, *324*, No. 121576.
(36) Zhang, L.; Li, M.; Liu, X.; Feng, J.; Liu, Y.; Tu, Y.; Li, S.; Duan, T. Fabrication of Amidoxime Grafted Polyacrylonitrile for Iodine Vapor Capture from Off-Gas. *Chem. Eng. J.* **2024**, *493*, No. 152618.
(37) Leng, R.; Sun, Y.; Wang, C.; Qu, Z.; Feng, R.; Zhao, G.; Han, B.; Wang, J.; Ji, Z.; Wang, X. Design and Fabrication of Hypercrosslinked Covalent Organic Adsorbents for Selective Uranium Extraction. *Environ. Sci. Technol.* **2023**, *57* (26), 9615−9626.
(38) Zhu, L.; Zhang, C.; Ma, F.; Bi, C.; Zhu, R.; Wang, C.; Wang, Y.; Liu, L.; Dong, H. Hierarchical Self-Assembled Polyimide Microspheres Functionalized with Amidoxime Groups for Uranium-Containing Wastewater Remediation. *ACS Appl. Mater. Interfaces* **2023**, *15* (4), 5577−5589.
(39) Xia, X.; Liao, Z.; Deng, J.; Yang, G.; Nie, X.; Ma, C.; Cheng, W.; Pan, N.; Zhang, W.; Dong, F. Efficient Purification of Low-Level Uranium-Containing Wastewater by Polyamine/Amidoxime Synergistically Reinforced Fiber. *Environ. Pollut.* **2024**, *344*, No. 123269.
(40) Yuan, K.; Ilton, E. S.; Antonio, M. R.; Li, Z.; Cook, P. J.; Becker, U. Electrochemical and Spectroscopic Evidence on the One-Electron Reduction of U(VI) to U(V) on Magnetite. *Environ. Sci. Technol.* **2015**, *49* (10), 6206−6213.
(41) Manos, M. J.; Ding, N.; Kanatzidis, M. G. Layered Metal Sulfides: Exceptionally Selective Agents for Radioactive Strontium Removal. *Proc. Natl. Acad. Sci. U. S. A.* **2008**, *105* (10), 3696−3699.
(42) Gabriel, B.; Teissié, J. Generation of Reactive-Oxygen Species Induced by Electropermeabilization of Chinese Hamster Ovary Cells and Their Consequence on Cell Viability. *Eur. J. Biochem.* **1994**, *223* (1), 25−33.
(43) Li, Z.; Yang, D.; Li, S.; Yang, L.; Yan, W.; Xu, H. Advances on Electrochemical Disinfection Research: Mechanisms, Influencing Factors and Applications. *Sci. Total Environ.* **2024**, *912*, No. 169043.
(44) Pandit, S.; Shanbhag, S.; Mauter, M.; Oren, Y.; Herzberg, M. Influence of Electric Fields on Biofouling of Carbonaceous Electrodes. *Environ. Sci. Technol.* **2017**, *51* (17), 10022−10030.
(45) Liu, X.; Xie, Y.; Hao, M.; Chen, Z.; Yang, H.; Waterhouse, G. I. N.; Ma, S.; Wang, X. Highly Efficient Electrocatalytic Uranium Extraction from Seawater over An Amidoxime-Functionalized In−N−C Catalyst. *Adv. Sci.* **2022**, *9* (23), No. 2201735.
(46) Feng, H.; Dong, H.; He, P.; He, J.; Hu, E.; Qian, Z.; Li, J.; Li, J.; Zhu, W.; Chen, T. Nickel Single Atom Mediated Phosphate Functionalization of Moss Derived Biochar Effectively Enhances Electrochemical Uranium Extraction from Seawater. *J. Mater. Chem. A* **2024**, *12* (13), 7896−7905.
(47) Amayri, S.; Arnold, T.; Reich, T.; Foerstendorf, H.; Geipel, G.; Bernhard, G.; Massanek, A. Spectroscopic Characterization of the Uranium Carbonate Andersonite $Na_2Ca[UO_2(CO_3)_3]\cdot 6H_2O$. *Environ. Sci. Technol.* **2004**, *38* (22), 6032−6036.
(48) Zhang, Z.; Dong, Z.; Wang, X.; Ying, D.; Niu, F.; Cao, X.; Wang, Y.; Hua, R.; Liu, Y.; Wang, X. Ordered Mesoporous Polymer−Carbon Composites Containing Amidoxime Groups for Uranium Removal from Aqueous Solutions. *Chem. Eng. J.* **2018**, *341*, 208−217.
(49) Wang, B.; Zhou, Y.; Li, L.; Wang, Y. Preparation of Amidoxime-Functionalized Mesoporous Silica Nanospheres (Ami-Msn) from Coal Fly Ash for the Removal of U(VI). *Sci. Total Environ.* **2018**, *626*, 219−227.
(50) Zhou, Y.; Li, Y.; Wang, X.; Liu, D.; Liu, D. Preparation of Amidoxime Functionalized Titanate Nanosheets for Efficient Extraction of Uranium from Aqueous Solution. *J. Solid State Chem.* **2020**, *290*, No. 121562.
(51) Wang, Y. H.; Xiang, Y. Q.; Huang, Q.; Yang, X. L.; Wang, S. L.; Zhou, Y. R.; Qin, S.; Gou, L. Q.; Tao, G. H.; He, L. High-Strength Ionic Hydrogel Constructed by Metal-Free Physical Crosslinking Strategy for Enhanced Uranium Extraction from Seawater. *Chem. Eng. J.* **2024**, *479*, No. 147875.
(52) Lines, A. M.; Hall, G. B.; Sinkov, S.; Levitskaia, T.; Gallagher, N.; Lumetta, G. J.; Bryan, S. A. Overcoming Oxidation State-Dependent Spectral Interferences: Online Monitoring of U(VI)

https://doi.org/10.1021/cbe.4c00141
Chem Bio Eng. 2025, 2, 53−63

Reduction to U(IV) Via Raman and UV−Vis Spectroscopy. *Ind. Eng. Chem. Res.* **2020**, *59* (19), 8894−8901.

https://doi.org/10.1021/cbe.4c00141
Chem Bio Eng. 2025, 2, 53−63